HHS Public Access

Author manuscript

Mitochondrion. Author manuscript; available in PMC 2020 January 24.

Published in final edited form as:

Mitochondrion. 2019 July ; 47: 244–255. doi:10.1016/j.mito.2018.12.004.

Hypoxia-reoxygenation of primary astrocytes results in a redistribution of mitochondrial size and mitophagy

Dominic D. Quintana, **Jorge A. Garcia**, **Saumyendra N. Sarkar**, **Sujung Jun**, **Elizabeth B. Engler-Chiurazzi**, **Ashley E. Russell**, **John Z. Cavendish**, **James W. Simpkins***

Center for Basic and Translational Stroke Research, Rockefeller Neuroscience Institute, West Virginia University, Morgantown, WV 26506, United States

Abstract

Astrocytes serve to maintain proper neuronal function and support neuronal viability, but remain largely understudied in research of cerebral ischemia. Astrocytic mitochondria are core participants in the metabolic activity of astrocytes. The objective of this study is to assess astrocyte mitochondrial competence during hypoxia and post-hypoxia reoxygenation and to determine cellular adaptive and pathological changes in the mitochondrial network. We hypothesize that during metabolic distress in astrocytes; mitochondrial networks undergo a shift in fission-fusion dynamics that results in a change in the morphometric state of the entire mitochondrial network. This mitochondrial network shift may be protective during metabolic distress by priming mitochondrial size and facilitating mitophagy. We demonstrated that hypoxia and post-hypoxia reoxygenation of rat primary astrocytes results in a redistribution of mitochondria to smaller sizes evoked by increased mitochondrial fission. Excessive mitochondrial fission corresponded to Drp-1 dephosphorylation at Ser 637, which preceded mitophagy of relatively small mitochondria. Reoxygenation of astrocytes marked the initiation of elevated mitophagic activity primarily reserved to the perinuclear region where a large number of the smallest mitochondria occurred. Although, during hypoxia astrocytic ATP content was severely reduced, after reoxygenation ATP content returned to near normoxic values and these changes mirrored mitochondrial superoxide production. Concomitant with these changes in astrocytic mitochondria, the number of astrocytic extensions declined only after 10-hours post-hypoxic reoxygenation. Overall, we posit a drastic mitochondrial network change that is triggered by a metabolic crisis during hypoxia; these changes are followed by mitochondrial degradation and retraction of astrocytic extensions during reoxygenation.

Keywords

Astrocytes; Mitochondria; Oxygen deprivation; Fission and fusion; Mitophagy; Drp-1; LC3

*Corresponding author at: Department of Physiology and Pharmacology, West Virginia University School of Medicine, One Medical Center Drive, Morgantown, WV 26501, United States., jwsimpkins@hsc.wvu.edu (J.W. Simpkins).

Author contribution statement

DDQ designed studies, conducted studies and composed the manuscript. JAG, SNS, SJ, EBE-C, AER, and JZC aided with studies, analyzed data, and revised the manuscript. JWS designed studies and revised the manuscript.

Conflict of interest

The authors declare no competing financial interest.

1. Introduction

Stroke is a cerebrovascular event characterized by severe cerebral ischemia that is the fifth leading cause of death and is the primary contributor of adult disability in the U.S. (Kochanek et al. 2014; Mozaffarian et al. 2015). During stroke there is a cerebral cellular energy crisis caused by a decline in the delivery of the substrates, glucose and molecular oxygen, resulting in a compromised synthesis of ATP through a collapse of oxidative phosphorylation and glycolysis (Rossi et al. 2007). Insufficient cellular ATP content interrupts a wide range of indispensable ATP-dependent processes, including ion balances across neuronal membranes (Hansen and Nedergaard 1988; Silver et al. 1997). An elevation of free cytosolic Ca^{2+} levels via voltage-gated and receptor-gated calcium channels is the central effector initiating the massive release of extracellular glutamate, and the primary cause of excitotoxicity in ischemia (Katayama et al. 1991; Duffy and MacVicar 1996; Parpura and Haydon 2000). Clearance of synaptic glutamate is a core function of astrocytes that helps protect against glutamate toxicity (Rothstein et al. 1996).

Also, astrocytes are critical for providing neurons with a source of glutamine necessary for glutamate production through a process known as the glutamate-glutamine cycle (Waniewski and Martin, 1986; Chaudhry et al. 2002). Embargo of glutamine delivery to neurons by the blockade of astrocytic conversion of glutamate to glutamine has been reported to reduce the potassium-evoked glutamate release in experimental models of focal ischemia, reducing infarct size (Paulsen and Fonnum 1989; Swanson et al. 1990). Astrocytic mitochondria are key organelles that allow astrocytes to participate in such extensive metabolic activities (Nehlig et al. 2004; Lovatt et al. 2007).

Here we investigated the effects of hypoxia and post-hypoxia reoxygenation on astrocytic mitochondrial structure, including mitochondrial dimensions and content, as well as the underlying mechanism(s) and functions of these dynamic changes. This research provides evidence of early mitochondrial fission during hypoxia-reoxygenation that may participate in the damaging effects of ischemic insult to the central nervous system.

2. Materials and methods

2.1. Preparation of primary astrocytic cultures

Primary astrocytic cultures were prepared using a method previously reported, which generated an 85% yield of astrocytes, and a 15%, and < 1% yield of progenitor cells and microglia, respectively (Almeida and Medina 1998). Embryonic day 19 pregnant rats were deeply anesthetized with isoflurane. After confirming deep anesthetization via tail pinch, rats received a 3-in. vertical incision to the lower abdomen. Once the incision was made, the embryos including the placenta and amniotic sacks were extracted from the uterus. Each embryo was removed from the amniotic sack by creating a small 0.5-cm incision and gently palpating the fetus out. As the fetuses were extracted from the amniotic sack, the heads were removed with sharp scissors and placed in ice cold HBSS buffer (HyClone, Thermo Fisher Scientific, Waltham, MA) while the remaining fetus were prepared. Fetal brains were removed by making a small incision across the sagittal suture. Once the brains were removed, the cerebellum was removed and discarded. The remaining brain tissue was

removed from the meninges with small forceps. The meninges free tissue was placed into a 50 mL centrifuge tube containing ice cold Dulbecco's modified Eagle's medium (DMEM) (HyClone, Thermo Fisher Scientific, Waltham, MA). Once all fetal brains were removed, the tissue was centrifuged at 10,000 times gravity for 3 min and subsequently resuspended in ice cold DMEM (HyClone, Thermo Fisher Scientific, Waltham, MA). Tissue was then minced by pipetting to dissociate aggregations of cells. Dissociated cells were then filtered through a 40-micron filter then cultured in DMEM (HyClone, Thermo Fisher Scientific, Waltham, MA) supplemented with 10% fetal bovine serum and 1% penicillin streptomycin for 7 days to allow sufficient time for cellular differentiation. After the growth phase, primary astrocytes were plated on 6 cm culture dishes, 96-well plates, or 6-well culture plates containing sterilized 22 × 22 mm glass cover-slips at a seeding density of 200,000, 10,000, and 50,000 cells per well, respectively. Primary astrocytes were allowed 24-h of growth before labeling procedure.

2.2. Hypoxia treatment and imaging preparation

Mitochondrial labeling preceded experimental treatment. Mitochondrial labeling in all three experimental conditions was done at the same time so that any time-relevant effects of the labeling procedure would occur uniformly. Mitochondrial labeling was performed with 70 nM of MitoTracker Red CMXRos (Invitrogen, Molecular Probes, Eugene, OR) diluted in prewarmed (37 °C) DMEM culture medium then allowed to incubate with primary astrocytes for 20 min before washing 2 times with prewarmed DMEM. Hypoxic treatment was administered as 0.4% oxygen in nitrogen gas balance (Airgas USA, LLC, St. Louis, MO) for 3 h while incubated at 37 °C. After the 3 h of hypoxia, primary astrocytes were removed from the hypoxic enclosure and allowed a 10-hour reoxygenation period at normoxic, atmospheric oxygen level. The experimental timeline was designed so that all experimental groups completed treatment at the same time. After treatment, coverslips containing astrocytes were washed once with 0.1 M phosphate buffer saline (PBS) at physiological pH then fixated with 3.7% paraformaldehyde at physiological pH for 15 min then subsequently washed 3 times with 0.1 M PBS for 5 min. After washing, free aldehyde groups were quenched with 0.3 M glycine in 0.1 M PBS at 7.4pH for 10 min followed by washing 2 times for 5 min. Coverslips containing astrocytes were mounted on glass specimen slides with a medium containing 3% polyvinyl alcohol/glycerin/Tris-HCl/DABCO.

2.3. Image acquisition and analysis

Microscopy images were acquired with a Zeiss LSM 510 violet confocal microscope with a 63× magnification oil objective running on a Zen platform. Several criteria were developed to select astrocytes for inclusion in the study. First, astrocytes were inspected and, astrocytes that did not show signs of imminent death or nascent apoptosis were selected; second, astrocytes had to show canonical morphology, including well-developed extensions and appropriate size; and third, astrocytes had to be adequately spaced apart so that a single astrocyte's boundaries could easily be determined. Seven normoxic, six hypoxic, and six hypoxic-reoxygenation astrocytes were selected from 3 cultures per group for a detailed assessment of mitochondria structure features. Image analysis was conducted with ImageJ software (ImageJ 1.48v, Wayne Rasband, National Institutes of Health, USA) using the

particle analysis function to provide mitochondrial estimates. The following parameters were determined: area distributions, length, diameter, area, total mitochondrial mass, and roundness. Mitochondrial size distributions were calculated by sorting the entire content of astrocytic mitochondria into specific area categories (0.004–0.79, 0.80–1.59, 1.60–2.39, 2.40–3.19, > 3.20 μm^2). Once the total number of mitochondria have been sorted into their respective size categories, the number of mitochondria that fell within each size range was counted; these numbers were used to calculate the percentage of total mitochondria that fall within each size range by dividing the sum of mitochondria per size range by the total number of mitochondria in the astrocyte. Mitochondrial mass was calculated by summating the total area of mitochondria for each astrocyte then dividing this by the number of astrocytes for that group. Mitochondrial aspect ratio (AR = major axis/minor axis) and form factor (FF = 1/4× (area/perimeter^2)) were used to describe the full array of mitochondrial size and complexity as previously reported (Koopman et al. 2005b). Average astrocytic area and astrocytic extensions were calculated to determine the effects of hypoxia and post-hypoxic reoxygenation on astrocytic morphology. Astrocytic extensions were classified into three categories, primary, secondary, and tertiary. Extensions with origins of the soma were deemed primary extensions, extensions with origins of primary extensions were termed secondary extensions, and extensions with origins of secondary extensions were termed tertiary extensions.

2.4. Three-dimensional surface reconstruction

Three-dimensional surface reconstructions of deconvolved primary z-stack data sets collected by confocal microscopy were generated by Imaris (Bitplane). *Z*-stacks were collected on a Zeiss LSM 710 confocal microscope running on the Zen 2 platform with a C-Apochromat 63×/1.20 objective. Parameters for z-stack image collection were as follows, a pinhole set to 0.7 Airy units, a frame size of 4096 × 4096, and a pixel dwell of 0.79 μs to generate 16-bit images with a digital zoom of 1. Images in z-stacks were set to be collected at a step size of 0.100 μm for the entire thickness of the cell.

2.5. Western blots

Primary astrocytes were cultured in 6 cm culture dishes (n = 5/group) in DMEM supplemented with 10% FBS and 1% penicillin streptomycin at a seeding density of ≈ 200,000 cells per dish. After 72-hours, astrocytes were either maintained at normoxia, exposed to 3-hours of hypoxia, or 3-hours hypoxia then 10-hours reoxygenation. To determine autophagic flux, an LC3 turnover assay was performed (Mizushima et al. 2010). Lysosomal degradation of LC3 II was inhibited by treating cells with 30 μM Chloroquine (Sigma-Aldrich, St. Louis, MO) diluted in DMEM prior to hypoxic exposure. Astrocytes treated with 10 μM forskolin or 10 μM rolipram were used as positive controls for phosphorylated Drp-1 at Ser637. After exposure, cells were lifted from culture dishes in 4 mL of 0.1 M PBS then collected into 15 mL conical tubes. Suspended cells were pelleted by centrifugation at 3000 rpm for 2-minutes. After centrifugation, supernatant was decanted and discarded. Primary astrocyte pellets were lysed with 250 μL RIPA buffer(0.5% deoxycholate/0.1% sodium dodecyl sulfate/150 mM sodium chloride/50 mM (pH 8.0) Tris-HCl) supplemented with 2 μL/mL protease and phosphatase inhibitors (EMD Millipore, Billerica, MA). Astrocytic lysates were then briefly sonicated then centrifuged at 12,000

rpm for 20-minutes to pellet cellular debris, supernatant was collected in new 2 mL microcentrifuge tubes. Protein concentrations were estimated using Pierce Protein Assay Reagent (Thermo Scientific, Rockford, IL) to normalize protein content variability between culture dishes. Lysates were prepared in 4× Laemmle buffer containing 10% β mercaptoethanol and placed in a heated water bath for 10-minutes to denature the protein samples. Protein samples were resolved by SDS-PAGE 4–20% precast gels, Mini-PROTEAN TGX (Bio Rad, USA) then transferred onto a PVDF Immunobilon membrane (EMD Millipore, Billerica, MA). Membranes were blocked with blocking buffer (LI-COR Bioscience, Lincoln, NE) supplemented with 0.1% Tween 20 for 45-minutes. Membranes were incubated with affinity purified primary antibodies raised in rabbit or mouse targeted against phosphorylateddynamin related protein 1 at Ser 637 (pDrp-1), Drp-1 (Cell Signaling, Danvers, MA), microtubule-associated 1A/1B-light chain 3 (LC3) (Sigma-Aldrich, St. Louis, MO), and β-actin (Santa Cruz Biotechnology, Dallas, TX) at a dilution of 1:500 for 24-hours at 4 °C. Membranes were washed 3 times for 15-minutes with TBST (20 mM Tris-HCl/500 mM NaCl/0.1% Tween 20) solution then incubated with IRDye 800CW and IRDaye 680RD (LI-COR Biosciences, Lincoln, NE) secondary goat antibodies targeted against rabbit or mouse IgG (Molecular Probes, Eugene, OR) for 4-hours. Blots were washed 5 times for 15-minutes with TBST then fluorescence imaged with an Odyssey imaging system (LI-COR Biosciences, Lincoln, NE). Blot images were analyzed using Image Studio Lite 4.0 (LI-COR Biosciences, Lincoln, NE) then analyzed for fluorescence intensity normalized to β-actin.

2.6. Mitochondrial autophagy measurement

Primary astrocytes were plated in 6-well culture plates containing 22 mm × 22 mm glass cover slips at a seeding density of 50,000 cells per well and incubated at 37 °C for 24-hours. Prior to hypoxic treatment, astrocytic mitochondria were labeled with 70 nM of MitoTracker Red CMXRos for 20-minutes then washed twice with pre-warmed (37 °C) DMEM culture medium. After receiving hypoxic or hypoxic reoxygenation treatment, cells were rinsed with ice-cold 0.1 M PBS at physiological pH then quickly fixated with 3.7% paraformaldehyde at physiological pH. Post-fixation, cells were washed 3 times for 5-minutes with 0.1 M PBS. Free aldehyde groups were quenched with 0.3 M glycine in 0.1 M PBS at a pH of 7.4 followed by washing 2 times for 5-minutes with 0.1 M PBS. Cells were then permeabilized with 0.025% Triton X-100 in PBS for 20-minutes and washed 3 times for 5-minutes with PBS. After permeabilization, cells were blocked with 2% BSA for 45-minutes. Cells were then incubated with affinity purified IgG primary antibodies targeted against LC3 raised in rabbit (Sigma-Aldrich, St. Louis, MO) at a dilution of 1:500 in a solution containing 1% BSA,0.01% Tween 20 in 0.1 M PBS for 24-hours. After incubation with primary antibodies, cells were washed 3 times for 5-minutes with PBS containing 0.01% tween 20. Cells were then incubated with Alexa 488 secondary goat antibodies targeted against rabbit IgG (Invitrogen, Carlsbad, CA). Alexa 488 secondary antibodies were diluted to 1:1000 in a solution containing 10% goat serum, 0.01% Tween 20 in PBS and allowed to incubate with the cells for 4-hours followed by 3 times wash for 5 min. Cells were counterstained with DAPI nuclear stain (Molecular Probes, Eugene, OR) then mounted with a medium containing 3% polyvinyl alcohol/glycerin/Tris-HCl/DABCO. Primary astrocytes were then imaged on a Zeiss LSM 710 violet confocal with a 63× magnification oil objective running

on the Zen 2 platform. Confocal micro-graphs were analyzed for immunofluorescence colocalization of LC3 with MitoTracker labeled mitochondria as an indication of nascent mitophagy. LC3-MitoTracker colocalization was used to calculate the percentage of mitochondria in each mitochondrial size range undergoing mitophagy. Confocal micrographs were also used to calculate immunofluorescence intensity as a function of distance from the nucleus as an indication of LC3 localization.

2.7. Mitochondrial ATP production

Mitochondrial ATP production was quantified using the CellTiter-Glo luminescent ATP assay kit (Promega, Madison WI) according to manufacturer's guidelines. Astrocytes were plated on 96-well black-walled assay plates and seeded at a density of 10,000 cells per well. After 24-hours of growth phase, cells received hypoxic treatment with or without reoxygenation and were allowed to equilibrate at room temperature for 30-minutes before the ATP assay was implemented. Luciferase luminescence was measured with a plate reader (BioTek). ATP was calculated in ng per 10,000 cells using an ATP standard curve. The standard curve was created immediately prior to running the assay to prevent ATP degradation. Standard curve was prepared by serial tenfold dilutions of ATP in DMEM.

2.8. Mitochondrial superoxide production

Time-dependent pre- and post-hypoxic reoxygenation associated superoxide $\left(O_2^-\right)$ production by mitochondria was measured with MitoSOX Red (Invitrogen), in accordance to manufacturer's guidelines. Measurements of O_2^- were recorded at 3-hours before hypoxic exposure and 0, 0.5, 1, 2, 4, 8, and 12-hours post-hypoxia, during the reoxygenation period. Primary astrocytes were plated on 96-well assay plates containing DMEM at a seeding density of 15,000 cells per well. Astrocytes were then cultured to 95–100% confluency before experimentation. 5-minutes prior to receiving MitoSOX Red, astrocyte DMEM media was replaced with HBSS media to conduct the assay. Each well containing astrocytes received 5 μM MitoSOX Red and allowed to incubate at 37° for 16-minutes. Fluorescence indication of O_2^- levels were detected via an excitation of 510 nm and emission of 580 nm with a plate reader (BioTek). Fluorescence intensity was detected by the plate reader and computed into mean fluorescence values, these values were then used to calculate the percentage change from normoxia for each time point.

2.9. Statistics

All data were obtained using cells from at least four different animals/preparations. Results are depicted as means +/− SEM for the number of determinants (n) for each of the three experimental groups (normoxia, 3-hours hypoxia, and 3-hours hypoxia then 10-hours reoxygenation). Statistical analysis used was either student's t-test or ANOVA, with Bonferroni or Dunnett post-hoc tests. Specific statistical analysis used in each experiment is noted in the individual figure legends. Bonferroni's multiple comparison analysis was used to compare all combinations of the three experimental groups. Dunnett's post hoc test was used for the comparison of the experimental groups with the normoxia group (control group). $p < 0.05$ was considered significant. The following number of astrocytes' mitochondria were quantified: 7 normoxic astrocytes, 6 hypoxic astrocytes, and 6 hypoxic-

reoxygenation astrocytes. For LC3 colocalization studies, the following number of astrocytes' mitochondria were quantified: 7 normoxic astrocytes, 5 hypoxic astrocytes, and 6 hypoxic-reoxygenation astrocytes.

3. Results

3.1. Mitochondrial size measurements

Astrocytic exposure to hypoxia demonstrated the dynamic ability of mitochondria to undergo fission and fusion in response to changes in environmental oxygen pressure (Fig. 1A and B). Hypoxic exposure for 3-hours with or without 10-hours reoxygenation resulted in a redistribution of mitochondrial size to a larger number of smaller mitochondria.

Primary astrocytes that were exposed to 3-hours hypoxia with no reoxygenation showed the largest redistribution to smaller sized mitochondria compared to the 3-hours hypoxia then 10-hours reoxygenation and normoxia groups (Fig. 1C). In the normoxia group, 35.86% of mitochondria fell within the 0.004–0.79 μm^2 range. After 3-hours of hypoxia these values increase to 64.59% ($p = 0.0004$) and after 10-hours of post-hypoxic reoxygenation the percentage of mitochondria that fell within the 0.004–0.79 μm^2 range remained significantly elevated at 54.03% ($p = 0.01$) compared to normoxia. This observed increase in smaller mitochondria was associated with an observed reduction of larger mitochondria falling within 1.6–2.39, 2.4–3.19, and > 3.2 μm^2 range (Fig. 1C). The average mitochondrial area differed between the groups; the normoxia group contained mitochondria with an average area of 1.69μm^2 compared with 0.86 μm^2 ($p < 0.01$) and 1.08 μm^2 ($p < 0.05$) for the 3-hours hypoxia and 3-hours hypoxia then 10-hours reoxygenation groups, respectively (Fig. 2A). Mitochondrial swelling is a known phenomenon associated with calcium-induced cytochrome-c release from mitochondria during instances of mitochondrial-induced apoptosis (Kobayashi et al. 2003; Ichimura 2011). To further make it clear that nascent cell death was absent during data collection and to determine if mitochondrial swelling contributes to the reported mitochondrial measurements, mitochondrial length and diameter were measured. Mitochondrial length was measured as the maximum distance between any two points within the mitochondrial boundaries. Mitochondrial diameter was measured as the minimum distance between two opposing points of mitochondrial boundaries. Astrocytes that were maintained under normoxia demonstrated a mean length of 2.70 μm compared to 1.29 μm ($p < 0.0001$) and 2.05 μm ($p < 0.0001$) after 3-hours of hypoxia and 10-hours post-hypoxic reoxygenation, respectively. Additionally, these data demonstrate a significant amelioration of mean mitochondrial length after 10-hours post-hypoxic reoxygenation ($p < 0.0001$) compared to 3-hours hypoxia, albeit significantly reduced compared to normoxia (Fig. 2B). In contrast to measurements of mitochondrial length, mitochondrial diameter did not depict any notable change between normoxia, 3-hours hypoxia, and 10-hours post-hypoxic reoxygenation (Fig. 2C).

Dephosphorylation of Drp-1 at Ser 637 by calcineurin is an essential step in mitochondrial fission (Cereghetti et al. 2008), and phosphorylation of Drp-1 at Ser 637 by PKA favors mitochondrial fusion (Chang and Blackstone 2007; Cribbs and Strack 2007). We therefore assessed Drp-1 phosphorylation at Ser 637 as percentage of total Drp-1 via Western blot analysis in primary astrocytes maintained under normoxia, 3-hours of hypoxia, and 10-hours

post-hypoxia reoxygenation. Our Western blot data revealed that astrocytes maintained under normoxic conditions contained 3.27% of total Drp-1 phosphorylated at Ser 637 whereas, astrocytes exposed to 3-hours of hypoxia contained 2.17% ($p = 0.0492$) of Drp-1 phosphorylated at Ser 637 compared to normoxia. After 10-hours of post-hypoxia reoxygenation, Drp-1 phosphorylation at Ser 637 increased to 4.92% ($p = 0.0058$) of control Drp-1 phosphorylation (Fig. 2D).

3.2. Mitochondrial population and mass

Interestingly, the total number of mitochondria per astrocyte was different among all three groups. In the normoxic control group, there were 79 mitochondria per astrocyte whereas the 3-hours hypoxia with no reoxygenation contained 124 mitochondria per astrocyte. However, after 10-hours of reoxygenation the number of mitochondria decreased to 52 per astrocyte ($p = 0.046$) compared to normoxia (Fig. 3A). To determine if the changes in mitochondrial population after hypoxia and reoxygenation affect the total mitochondrial content in astrocytes, we calculated the total mitochondrial area per astrocyte. Astrocytes that were maintained at normoxia contained a total mitochondrial area of 123 μm^2; however, following 3-hours of hypoxia the total mitochondrial area was reduced to 102 μm^2 and after 10-hours reoxygenation the total mitochondrial area was further reduced to 57 μm^2 ($p = 0.0218$) compared to normoxia (Fig. 3B).

3.3. Mitochondrial fragmentation

Rounded mitochondria are indicative of fragmentation (Brustovetsky et al. 2009) and cellular stress (Dubinsky and Levi 1998). Therefore, we measured mitochondrial roundness to assess the extent of mitochondrial fragmentation. These data are depicted on a scale from 0 to 1; 1 being a perfect circle. Notably, astrocytes exposed to hypoxia displayed an alteration of mitochondrial morphology to a more rounded shape. Astrocytes that were maintained under normoxia contained mitochondria that scored an average of 0.36 on the roundness index. After 3-hours of hypoxia this score increased to 0.53 ($p = 0.0001$) then decreased to 0.50 ($p = 0.0001$) after 10-hours of reoxygenation (Fig. 4A). A reduction of mitochondrial network complexity can result from fragmented mitochondria and increased mitochondrial fission. Therefore, mitochondrial aspect ratio (AR) and form factor (FF) was calculated to describe mitochondrial network complexity. Mitochondria that measure greater AR are larger mitochondria whereas mitochondria that score greater on FF contain more complex branching (Koopman et al. 2005a, 2005b). Under normoxic conditions, mitochondria demonstrated an AR and FF of 4.49 and 2.58, respectively. After hypoxia exposure, the AR and FF decreased to 2.06 and 1.44, respectively indicating less complex mitochondrial networks. Furthermore, 10-hours of post-hypoxic reoxygenation resulted in a slight amelioration of both AR (3.03) and FF (1.83) (Fig. 4A–D).

3.4. Mitochondrial autophagy

Excessive mitochondrial fragmentation may predispose mitochondria to loss of membrane potential and buffering capacity resulting in mitochondria being targeted for autophagy (Ishihara et al. 2003; Legros et al. 2003). Therefore, we next determined the extent of mitochondrial autophagy after exposure to hypoxia and post-hypoxia reoxygenation and further to determine if smaller mitochondria are targeted for autophagy. During autophagy,

cytosolic LC3 I is cleaved then lipidated before being inserted as LC3 II into the autophagosome membrane (Tanida et al. 2004). We first measured the conversion of LC3 I into LC3 II by calculating the ratio of LC3 II/(LC3 I + LC3 II) (Mizushima and Yoshimori 2007) via Western blot to determine the effects of hypoxia and post hypoxia reoxygenation on the number of autophagosomes. Astrocytes exposed to 3-hours hypoxia then 10-hours reoxygenation showed an RFU (relative fluorescence unit) of 0.436 ($p < 0.0001$) conversion to LC3 II compared to 0.316 and 0.194 LC3 II conversion in the 3-h hypoxia and normoxia groups, respectively (Fig. 5A-B). Changes in LC3 II corresponded with a decrease in VDAC to 0.728 ($p < 0.02$) and 0.803 ($p < 0.05$) fold of normoxia in astrocytes exposed to 3-hours hypoxia and 3-hours hypoxia then 10-hours reoxygenation, respectively (Fig. 5C). We next performed an LC3 turnover assay to determine autophagic flux as an indication of autophagic induction (Mizushima and Yoshimori 2007; Klionsky et al. 2008; Rubinsztein et al. 2009; Mizushima et al. 2010). The measurement of autophagic flux is centered on the notion that LC3 II is degraded in the autolysosome during autophagy. The LC3 turnover assay was performed by inhibiting lysosomal acidification with 30 μM chloroquine prior to cells receiving hypoxic exposure. Astrocytes maintained at normoxia demonstrated an LC3 II turnover at 2.54 compared to 4.01 ($p < 0.006$) and 7.91 ($p < 0.0001$) in astrocytes exposed to 3-hours hypoxia and 3-hours hypoxia then 10-hours reoxygenation, respectively (Fig. 5D). In addition, under normoxic conditions, LC3 II was 204.04% ($p < 0.0009$) greater in astrocytes treated with 30 μM chloroquine compared to astrocytes that were not treated with chloroquine (Fig. 5E). These data demonstrating differences in LC3 II levels under basal conditions (normoxia) between astrocytes treated with chloroquine and without chloroquine rule out blocked autophagic processing as a contributor to LC3 II accumulation in our data (Fig. 5E).

Mitochondrial autophagy was assessed via immunofluorescence colocalization of LC3 and MitoTracker after hypoxia and post hypoxia reoxygenation. Confocal micrographs were collected from astrocytes maintained at normoxia, 3-hours hypoxia, and 10-hours post-hypoxic reoxygenation. As a positive control group, astrocytes maintained under normoxia were treated with 10uM FCCP to induce mitochondrial autophagy (Fig. 5F). The confocal micrographs were used to create colormap representative images demonstrating colocalized mitochondria with LC3. The colormap images were used to calculate the percentage of mitochondria targeted for autophagy (Fig. 5G), the size of mitochondria primarily affected by mitophagy (Fig. 5H), and the cellular localization of mitochondrial autophagic activity (Fig. 5I). Our colocalization analysis indicated that under normoxic conditions 26.4% of total mitochondria are targeted for mitophagy compared to 24.9% and ($p < 0.01$) 43.7% of mitochondria in astrocytes incubated under hypoxia for 3-hours and 3-hours hypoxia then 10-hours reoxygenation, respectively. In the positive control group, astrocytes treated with FCCP and maintained under normoxia contained 56.1% of their total mitochondria targeted for mitophagy. Our data indicate that the smallest mitochondria ranging in size of 0.004–0.79μm^2 were most targeted by mitophagy. Astrocytes maintained under normoxia contained 3.68% of the smallest mitochondria targeted for mitophagy. Whereas, astrocytes exposed to 3-hours of hypoxia contained 7.23% ($p < 0.0001$) of the smallest mitochondria targeted for mitophagy. After 10-hours post-hypoxic reoxygenation the percentage of smallest mitochondria targeted for mitophagy increased to 17.45% ($p < 0.0001$). Mitochondria falling

within the size rage of 0.80–1.59μm^2 contained the second largest number of mitochondria targeted for mitophagy; these mitochondria represented the second-to smallest mitochondria. Astrocytes maintained under normoxia contained 6.59% of small mitochondria targeted for mitophagy. Whereas, astrocytes exposed to 3-hours of hypoxia contained 5.63% of small mitochondria targeted for mitophagy. After 10-hours of post-hypoxic reoxygenation the percentage of small mitochondria targeted for mitophagy significantly increased to 12.65% ($P < 0.05$). Additionally, our data suggests that the majority of mitochondrial autophagic activity occurs at specific cellular locations during hypoxia and post-hypoxic reoxygenation. Astrocytes exposed to 3-hours of hypoxia then 10-hours reoxygenation showed increased LC3 fluorescence intensity near the nucleus compared to the approximate homogenous distribution of LC3 fluorescence intensity in astrocytes exposed to 3-hours of hypoxia or normoxia.

3.5. Mitochondrial ATP production

Hypoxia induces mitochondrial respiratory inhibition resulting in a rapid decline of astrocytic ATP production. Astrocytes maintained under normoxia contained 52.89 ng of ATP per 10,000 cells. After 3-hours of hypoxic exposure astrocytic ATP content declined to 23.1 ng ($p < 0.0001$) per 10,000 cells. Interestingly, after 10-hours of post-hypoxic reoxygenation, astrocytes demonstrated a significant amelioration of ATP content to 47.12 ng per 10,000 ($p < 0.0001$) although still significantly below ATP content of astrocytes maintained under normoxia ($p < 0.0001$) (Fig. 6A).

3.6. Mitochondrial superoxide production

Mitochondrial superoxide production is a major contributor of cellular damage via oxidation of lipids, proteins, and other biomolecules. Mitochondrial superoxide production occurs at complex I and III of the mitochondrial electron transport chain, with the majority of superoxide production occurring at complex I via reversal of electron transport during cerebral ischemia (Liu et al. 2002; Talbot et al. 2004). To determine the levels of superoxide generation by mitochondria, a fluorescence probe, MitoSOX Red, was used during normoxia, hypoxia, and subsequent time-periods of post-hypoxia reoxygenation. Our data indicates that astrocytes maintained under normoxia contained the highest levels of mitochondrial superoxide relative to hypoxia and post-hypoxia reoxygenation. At the conclusion of 3-hours hypoxic exposure, superoxide content reduced to 27.39% of the superoxide observed in normoxic astrocytes. After the first 30-minutes of post-hypoxic reoxygenation, astrocytic superoxide content increased to 56.71% of normoxic values. Furthermore, as post-hypoxic reoxygenation progressed, astrocytic superoxide production continued to increase to 60.72%, 67.65%, and 73.34% of normoxic superoxide content after 1-, 2, and 4-hours of reoxygenation, respectively. Interestingly, after 8-hours of post-hypoxic reoxygenation, astrocytic superoxide production reached a peak of 89.65% of normoxic values followed by a decline to 82.55% after 12-hours of post-hypoxic reoxygenation (Fig. 6B).

3.7. Astrocytic extensions and swelling

Astrocytic extensions are structures that participate in critical cellular processes that mediate metabolic support to neurons, neurovascular coupling, and neurotransmitter recycling.

Hypoxia and post-hypoxia reoxygenation induced a loss of astrocytic extensions. Astrocytes maintained under normoxia contained an average of 40 extensions. However, after exposure to 3-hours of hypoxia, astrocytic extensions declined to an average of 31 and after 10-hours of post-hypoxic reoxygenation, astrocytic extensions further declined to an average of 21 ($p < 0.05$) (Fig. 7A-D). We next determined the specific branch level of extension loss in these astrocytes. To determine the specific branch level of extension loss, each astrocytic extension was categorized based on branch origin. Extensions with origins of the soma were deemed primary extensions, extensions with origins on primary extensions were termed secondary extensions, and extensions with origins on secondary extensions were termed tertiary extensions. Our data revealed significant secondary and tertiary astrocyte extension loss. Astrocytes maintained under normoxia demonstrated the most complex branch patterning indicated by a higher number of secondary and tertiary extensions (Fig. 7A and D). Normoxic astrocytes contained an average of 15 primary, 20 secondary, and 4 tertiary astrocytic extensions. However, after exposure to 3-hours of hypoxia, astrocytes demonstrated marked loss of extension density (Fig. 7B and E). Astrocytes exposed to 3-hours of hypoxia contained 16 primary, 12 secondary, and 2 tertiary astrocytic extensions. After 10-hours of post-hypoxic reoxygenation, astrocyte extension loss was clearly recognizable, in both density and complexity (Fig. 7C and E). Astrocytes exposed to 3-hours hypoxia then 10-hours reoxygenation contained 10 primary ($p = 0.0432$), 8 secondary ($p = 0.0063$), and 0.5 tertiary ($p = 0.0145$) astrocytic extensions (Fig. 7C and E). Lastly, we observed evidence of astrocyte swelling during hypoxic exposure. This swelling did not persist throughout the reoxygenation phase of hypoxic exposure. Astrocytes maintained under normoxia contained an average astrocytic area of 1677.03 μm^2. However, after hypoxic incubation, astrocytic area significantly increased to 3076.01 μm^2 ($p = 0.0425$). Following 10-hours post-hypoxia reoxygenation, astrocytic area reduced to 1487.22 μm^2. These changes in astrocytic area indicate astrocyte swelling during hypoxic exposure that does not persist on to the reoxygenation phase of exposure (Fig. 7F). Furthermore, our cell death assay of astrocytes exposed to 3-hours of hypoxia and 10-hours post-hypoxic reoxygenation (Fig. 7G) indicated no change in astrocyte viability, suggesting that these observed changes in astrocytic swelling did not result in cellular death.

4. Discussion

In this study, we have demonstrated that hypoxia and post-hypoxia reoxygenation of primary astrocytes results in a redistribution of mitochondria to smaller sizes evoked by an increase in mitochondrial fission. Excessive mitochondrial fission corresponded to Drp-1 dephosphorylation at Ser 637, which preceded mitophagy of relatively small mitochondria. Post-hypoxia reoxygenation of astrocytes marked the initiation of elevated mitophagic activity particularly in the perinuclear region where a large number of the smallest mitochondria were undergoing nascent degradation. Although, during hypoxia astrocytic ATP content severely reduced, after reoxygenation ATP content returned to near normoxic values; these changes were observed in mitochondrial superoxide production as well. Concomitant with these mitochondrial morphological and functional changes in astrocytes, the number of astrocytic extensions declined particularly after 10-hours post-hypoxic reoxygenation. Overall, we posit a drastic mitochondrial network change that is triggered by

a metabolic crisis during hypoxia; these changes are followed by mitochondrial degradation and retraction of astrocytic extensions.

Reports concerning mitochondrial fusion and fission as being beneficial or detrimental to cell function and viability have been considerably disparate (Chang and Blackstone 2007; Estaquier and Arnoult 2007; Parone et al. 2008; Ong et al. 2010; Gomes et al. 2011; Chou et al. 2012; Papanicolaou et al., 2012; Qi et al. 2013). However, it is well established that asymmetric mitochondrial fission is an important event central to mitochondrial quality control that eliminates damaged or dysfunctional parts of mitochondria (Twig et al. 2008). We demonstrated that hypoxia results in a rapid redistribution of mitochondria to smaller sizes (Fig. 1). Mitochondrial damage is an event of the reoxygenation phase of ischemic injury (Kowaltowski and Vercesi 1999). Accordingly, our data indicated no increase in LC3 II conversion or elevations in LC3-targeted mitochondria in astrocytes maintained under hypoxia. In addition, the absence of mitophagic activity during hypoxia in astrocytes further suggests that the observed fission is independent of the organelle recycling that occurs during conditions of macromolecule depletion (Kristensen et al. 2008; Hailey et al. 2010; Egan et al. 2011). The most probable cause of mitochondrial fission during hypoxia is the onset of a metabolic crisis resulting from a rapid and severe ATP depletion. An inverse correlation between mitochondrial size and metabolic competence has been described in the rat brain (Bertoni-Freddari et al. 2003). This may explain our data suggesting that larger mitochondria predominantly undergo fission, increasing the amount of smaller mitochondria during hypoxia and throughout reoxygenation. Therefore, we predict that during hypoxia an astrocytic metabolic crisis triggers mitochondrial fission as a functional means of increasing energy production by mitochondria.

It is well accepted that considerable cellular damage occurs during the reperfusion phase of ischemic injury (Kalogeris et al. 2012). A major contributor to ischemic-reperfusion injury is the mitochondrial production of superoxide at complex I (Arroyo et al. 1987; Bolli et al. 1989; Chouchani et al. 2013). Mitochondrial ROS production during initial ischemia reperfusion is driven by the rapid oxidation of succinate by the mitochondrial respiratory complex succinate dehydrogenase and reversal of electron transport (Chouchani et al. 2014). While this may devastate neuronal viability, astrocytes demonstrate increased tolerance to oxidative stress relative to neurons (Sochocka et al. 1994; Bolaños et al. 1995). Astrocyte tolerance to oxidative stress has been suggested to be an effect of greater metabolic plasticity (Escartin et al. 2007; Halim et al. 2010), more robust antioxidant buffering capacity (Dringen et al. 2000; Shih et al. 2003; Belanger and Magistretti 2009), and a lesser dependence of ATP production via oxidative phosphor-ylation (Marrif and Juurlink 1999; Solaini and Harris, 2005). Our data depict a progressive increase in mitochondrial superoxide production throughout the reoxygenation phase of astrocytes exposed to hypoxia, which occurred with no notable ROS burst. This gradual recovery of superoxide production parallels the oxidative phosphorylation rate of these mitochondria (Perez-Campo et al. 1998; Balaban et al. 2005). The absence of an ROS burst may explain astrocyte resistance to hypoxiareoxygenation-induced cell death.

We provide evidence for two morphological responses of astrocytes to hypoxia. First, during hypoxia, we observed astrocytic swelling that did not persist throughout the reoxygenation

phase. Astrocytic swelling is a known phenomenon of cerebral ischemia and possibly contributes to ischemic injury, including excitotoxicity, extracellular ionic dysregulation, and compressive damage to dendrites (Kimelberg et al. 1995; Kimelberg 2004; Risher et al. 2012). This astrocytic swelling has been attributed to elevated cytosolic calcium concentration independent of mitochondrial depolarization (Kahlert and Reiser 2002) in models of cerebral ischemia (Duffy and MacVicar 1996; Brookes et al. 2004). The maintenance of homeostatic parameters of ion concentrations in astrocytes is dependent on ATP availability. Accordingly, our data show both a decline in astrocytic ATP content and swelling of astrocytes during hypoxia suggesting insufficient ATP availability for maintaining ionic homeostasis. Ultimately, astrocytic swelling and its regulatory mechanism render astrocytes depolarized (Kimelberg and O'Connor, 1988). This in mind, astrocyte morphology is clearly intimately coupled and acutely sensitive to the competence of cellular ATP production.

In addition to swelling, we also provide evidence for a robust retraction of secondary and tertiary astrocytic extensions after hypoxiareoxygenation exposure. Astrocytic extensions are key structures enriched in excitatory amino acid transporters such as GLT-1, along with other surface receptors participating in homeostatic processes such as neurovascular coupling, translocation of specific molecules across the blood brain barrier, and maintenance of extracellular milieu.

During the energy crisis following ischemia, astrocytic ATP content is insufficient to support astrocyte relevant processes let alone fulfilling the energy requirement for astrocyte-mediated processes to neurons, which may account for some of the pathophysiological mechanism that degenerate neurons which are strongly thought to be prevented by astrocytic function.

A report by O'Donnell et al. (O'Donnell et al. 2016) provided work consistent with our data in that, oxygen glucose deprivation (OGD) of hippocampal slice cultures resulted in a reduction of astrocytic mitochondrial length and occupancy (area). Furthermore, in agreement with our measurements of LC3 II (LC3 B) after hypoxia with no reoxygenation, O'Donnell and colleagues provide similar observations of a negligible change in LC3 B content with as much as 24-h of OGD (O'Donnell et al. 2016). Importantly, our data depict a strong increase of LC3 B content occurring only with post-hypoxia reoxygenation suggesting that the bulk of mitochondrial autophagy occurs during the reoxygenation phase with hypoxic exposure. Therefore, pharmacological inhibition of mitochondrial autophagy in studies designed to investigate the effects of OGD on mitochondria occupancy would best be administered during a reoxygenation phase of OGD insult.

In summary, our data indicate a rapid metabolic crisis that ensues during hypoxia of astrocytes that is associated with reduced ATP production, a shift in mitochondrial distribution to smaller sizes, a loss of mitochondrial complexity, a reduction in mitochondrial superoxide production, and astrocytic swelling. During post-hypoxic-reoxygenation, there is a reduction in mitochondrial number mediated by smaller mitochondria targeted by mitophagy, a recovery of ATP production, restoration of mitochondrial superoxide production, and a general loss of astrocytic extensions.

Acknowledgements

This work was supported by NIH grants P20 GM109098, P01 AG027956, U54 GM104942 and T32 AG052375. Imaging experiments and image analysis were performed in the West Virginia University Microscope Imaging Facility, which has been supported by the Mary Babb Randolph Cancer Center and NIH grants T32 AG052375, P20 RR016440, P30 RR032138/GM103488 and P20 RR016477.

References

Almeida A, Medina JM, 1998 A rapid method for the isolation of metabolically active mitochondria from rat neurons and astrocytes in primary culture. Brain Res. Protocol 2, 209–214.

Arroyo CM, Kramer JH, Dickens BF, Weglicki WB, 1987 Identification of free radicals in myocardial ischemia/reperfusion by spin trapping with nitrone DMPO. FEBS Lett. 221, 101–104. [PubMed: 3040465]

Balaban RS, Nemoto S, Finkel T, 2005 Mitochondria, oxidants, and aging. Cell 120,483–495. [PubMed: 15734681]

Belanger M, Magistretti PJ, 2009 The role of astroglia in neuroprotection. DialoguesClin. Neurosci 11, 281–296.

Bertoni-Freddari C, Fattoretti P, Paoloni R, Caselli U, Giorgetti B, Solazzi M, 2003 Inverse correlation between mitochondrial size and metabolic competence: a quantitative cytochemical study of cytochrome oxidase activity. Naturwissenschaften 90, 68–71. [PubMed: 12590300]

Bolaños JP, Heales SJ, Land JM, Clark JB, 1995 Effect of peroxynitrite on the mitochondrial respiratory chain: differential susceptibility of neurones and astrocytes in primary culture. J. Neurochem 64, 1965–1972. [PubMed: 7722484]

Bolli R, Jeroudi MO, Patel BS, Dubose CM, Lai EK, Roberts R, McCay PB, 1989 Direct evidence that oxygen-derived free radicals contribute to postischemic myocardial dysfunction in the intact dog. Proc. Natl. Acad. Sci. U. S. A 86, 4695–4699. [PubMed: 2543984]

Brookes PS, Yoon YS, Robotham JL, Anders MW, Sheu SS, 2004 Calcium, ATP, and ROS: a mitochondrial love-hate triangle. Am. J. Physiol. Physiol 287, C817–C833.

Brustovetsky T, Li V, Brustovetsky N, 2009 Stimulation of glutamate receptors in cultured hippocampal neurons causes Ca2+−dependent mitochondrial contraction. Cell Calcium 46, 18–29. [PubMed: 19409612]

Cereghetti GM, Stangherlin A, Martins de Brito O, Chang CR, Blackstone C,Bernardi P, Scorrano L, 2008 Dephosphorylation by calcineurin regulates translocation of Drp1 to mitochondria. Proc. Natl. Acad. Sci. U. S. A 105, 15803–15808. [PubMed: 18838687]

Chang C-R, Blackstone C, 2007 Cyclic AMP-dependent protein kinase phosphorylation of Drp1 regulates its GTPase activity and mitochondrial morphology. J. Biol. Chem 282, 21583–21587. [PubMed: 17553808]

Chaudhry FA, Schmitz D, Reimer RJ, Larsson P, Gray AT, Nicoll RA,Kavanaugh M, Edwards RH, 2002 Glutamine uptake by neurons: interaction of protons with system a transporters. J. Neurosci 22, 62–72. [PubMed: 11756489]

Chou CH, Lin CC, Yang MC, Wei CC, De, Liao H, Lin RC, Tu WY, Kao TC, Hsu CM, Cheng JT, Chou AK, Lee CI, Loh JK, Howng SL, Hong YR, 2012 GSK3beta-mediated Drp1 phosphorylation induced elongated mitochondrial morphology against oxidative stress. PLoS One 7.

Chouchani ET, Methner C, Nadtochiy SM, Logan A, Pell VR, Ding S, James AM, Cochemé HM, Reinhold J, Lilley KS, Partridge L, Fearnley IM, Robinson AJ, Hartley RC, Smith RAJ, Krieg T, Brookes PS, Murphy MP, 2013 Cardioprotection by S-nitrosation of a cysteine switch on mitochondrial complex I. Nat. Med 19, 753–759. [PubMed: 23708290]

Chouchani ET, Pell VR, Gaude E, Aksentijević D, Sundier SY, Robb EL, Logan A, Nadtochiy SM, Ord ENJ, Smith AC, Eyassu F, Shirley R, Hu C-H, Dare AJ, James AM, Rogatti S, Hartley RC, Eaton S, Costa ASH, Brookes PS, Davidson SM, Duchen MR, Saeb-Parsy K, Shattock MJ, Robinson AJ, Work LM, Frezza C, Krieg T, Murphy MP, 2014 Ischaemic accumulation of succinate controls reperfusion injury through mitochondrial ROS. Nature 515, 431–435. [PubMed: 25383517]

Cribbs JT, Strack S, 2007 Reversible phosphorylation of Drp1 by cyclic AMP-dependent protein kinase and calcineurin regulates mitochondrial fission and cell death. EMBO Rep. 8, 939–944. [PubMed: 17721437]

Dringen R, Gutterer JM, Hirrlinger J, 2000 Glutathione metabolism in brain:Metabolic interaction between astrocytes and neurons in the defense against reactive oxygen species. Eur. J. Biochem 267, 4912–4916. [PubMed: 10931173]

Dubinsky JM, Levi Y, 1998 Calcium-induced activation of the mitochondrial permeability transition in hippocampal neurons. J. Neurosci. Res 53, 728–741. [PubMed: 9753200]

Duffy S, MacVicar B.a., 1996 In vitro ischemia promotes calcium influx and intracellular calcium release in hippocampal astrocytes. J. Neurosci 16, 71–81. [PubMed: 8613811]

Egan DF, Shackelford DB, Mihaylova MM, Gelino S, Kohnz RA, Mair W,Vasquez DS, Joshi A, Gwinn DM, Taylor R, Asara JM, Fitzpatrick J, Dillin A, Viollet B, Kundu M, Hansen M, Shaw RJ, 2011 Phosphorylation of ULK1 (hATG1) by AMP-activated protein kinase connects energy sensing to mitophagy. Science 331, 456–461. [PubMed: 21205641]

Escartin C, Pierre K, Colin A, Brouillet E, Delzescaux T, Guillermier M, Dhenain M, Déglon N, Hantraye P, Pellerin L, Bonvento G, 2007 Activation of astrocytes by CNTF induces metabolic plasticity and increases resistance to metabolic insults. J. Neurosci 27, 7094–7104. [PubMed: 17611262]

Estaquier J, Arnoult D, 2007 Inhibiting Drp1-mediated mitochondrial fission selectively prevents the release of cytochrome c during apoptosis. Cell Death Differ. 14, 1086–1094. [PubMed: 17332775]

Gomes LC, Di Benedetto G, Scorrano L, 2011 During autophagy mitochondria elongate, are spared from degradation and sustain cell viability. Nat. Cell Biol 13, 589–598. [PubMed: 21478857]

Hailey DW, Rambold AS, Satpute-Krishnan P, Mitra K, Sougrat R, Kim PK,Lippincott-Schwartz J, 2010 Mitochondria supply membranes for autophagosome biogenesis during starvation. Cell 141, 656–667. [PubMed: 20478256]

Halim ND, Mcfate T, Mohyeldin A, Okagaki P, Korotchkina LG, Patel MS,Jeoung NH, Harris RA, Schell MJ, Verma A, 2010 Phosphorylation status of pyruvate dehydrogenase distinguishes metabolic phenotypes of cultured rat brain astrocytes and neurons. Glia 58, 1168–1176. [PubMed: 20544852]

Hansen AJ, Nedergaard M, 1988 Brain ion homeostasis in cerebral ischemia. Neurochem. Pathol. 9, 195–209. [PubMed: 3247069]

Ichimura T, 2011 Involvement of mitochondrial swelling in cytochrome c release from mitochondria treated with calcium and Alloxan. J. Biophys. Chem 2, 10–18.

Ishihara N, Jofuku A, Eura Y, Mihara K, 2003 Regulation of mitochondrial morphology by membrane potential, and DRP1-dependent division and FZO1-dependent fusion reaction in mammalian cells. Biochem. Biophys. Res. Commun 301, 891–898. [PubMed: 12589796]

Kahlert S, Reiser G, 2002 Swelling of mitochondria in cultured rat hippocampal astrocytes is induced by high cytosolic Ca2+ load, but not by mitochondrial depolarization. FEBS Lett. 529, 351–355. [PubMed: 12372627]

Kalogeris T, Baines CP, Krenz M, Korthuis RJ, 2012 Cell Biology of Ischemia/Reperfusion Injury.

Katayama Y, Kawamata T, Tamura T, Hovda DA, Becker DP, Tsubokawa T, 1991 Calcium-dependent glutamate release concomitant with massive potassium flux during cerebral ischemia in vivo. Brain Res. 558, 136–140. [PubMed: 1682012]

Kimelberg HK, 2004 Increased release of excitatory amino acids by the actions of ATP and peroxynitrite on volume-regulated anion channels (VRACs) in astrocytes. Neurochem. Int 45, 511–519. [PubMed: 15186917]

Kimelberg HK, O'Connor E, 1988 Swelling of astrocytes causes membrane potential depolarization. Glia 1219–1224.

Kimelberg HK, Rutledge E, Goderie S, Charniga C, 1995 Astrocytic swelling due to hypotonic or high K+ medium causes inhibition of glutamate and aspartate uptake and increases their release. J. Cereb. Blood Flow Metab 15, 409–416. [PubMed: 7713998]

Klionsky DJ, Abeliovich H, Agostinis P, Agrawal DK, Aliev G, Askew DS, Baba M, Baehrecke EH, Bahr BA, Ballabio A, Bamber BA, Bassham DC, Bergamini E, Bi X, Biard-Piechaczyk M, Blum JS, Bredesen DE, Brodsky JL, Brumell JH, Brunk UT, Bursch W, Camougrand N, Cebollero E,

Cecconi F, Chen Y, Chin L-S, Choi A, Chu CT, Chung J, Clarke PGH, Clark RSB, Clarke SG, Clave C, Cleveland JL, Codogno P, Colombo MI, Coto-Montes A, Cregg JM, Cuervo AM, Debnath J, Demarchi F, Dennis PB, Dennis PA, Deretic V, Devenish RJ, Di Sano F, Dice JF, Difiglia M, Dinesh-Kumar S, Distelhorst CW, Djavaheri-Mergny M, Dorsey FC, Droge W, Dron M, Dunn WAJ, Duszenko M, Eissa NT, Elazar Z, Esclatine A, Eskelinen E-L, Fesus L, Finley KD, Fuentes JM, Fueyo J, Fujisaki K, Galliot B, Gao F-B, Gewirtz DA, Gibson SB, Gohla A, Goldberg AL, Gonzalez R, Gonzalez-Estevez C, Gorski S, Gottlieb RA, Haussinger D, He Y-W, Heidenreich K, Hill JA, Hoyer-Hansen M, Hu X, Huang W-P, Iwasaki A, Jaattela M, Jackson WT, Jiang X, Jin S, Johansen T, Jung JU, Kadowaki M, Kang C, Kelekar A, Kessel DH, Kiel JAKW, Kim HP, Kimchi A, Kinsella TJ, Kiselyov K, et al., 2008 Guidelines for the use and interpretation of assays for monitoring autophagy in higher eukaryotes. Autophagy 4, 151–175. [PubMed: 18188003]

Kobayashi T, Kuroda S, Tada M, Houkin K, Iwasaki Y, Abe H, 2003 Calcium-induced mitochondrial swelling and cytochrome c release in the brain: its biochemical characteristics and implication in ischemic neuronal injury. Brain Res. 960, 62–70. [PubMed: 12505658]

Kochanek KD, Murphy SL, Xu MDJ, Arias Ph.D.E, 2014 Mortality in the United States, 2013. In: NCHS Data Brief. 178 pp. 7.

Koopman WJH, Verkaart S, Visch HJ, van der Westhuizen FH, Murphy MP, van den Heuvel L, Smeitink JAM, Willems P, 2005a Inhibition of complex I of the electron transport chain causes O-2(−)center dot-mediated mitochondrial outgrowth. Am. J. Physiol. Physiol 288, C1440–C1450.

Koopman WJH, Visch H-J, Verkaart S, van den Heuvel LWPJ, Smeitink JA,M, Willems PHGM, 2005b Mitochondrial network complexity and pathological decrease in complex I activity are tightly correlated in isolated human complex I deficiency. Am. J. Phys. Cell Phys 289, C881–C890.

Kowaltowski AJ, Vercesi AE, 1999 Mitochondrial damage induced by conditions of oxidative stress. Free Radic. Biol. Med 26, 463–471. [PubMed: 9895239]

Kristensen AR, Schandorff S, Høyer-Hansen M, Nielsen MO, Jäättelä M, Dengjel J, Andersen JS, 2008 Ordered organelle degradation during starvation-induced autophagy. Mol. Cell. Proteomics 7, 2419–2428. [PubMed: 18687634]

Legros F, Lombès A, Frachon P, Rojo M, 2003 Mitochondrial fusion in human cells is efficient, requires the inner membrane potential, and is mediated by mitofusins. Mol. Biol. Cell 14, 2559–2569. [PubMed: 12808051]

Liu Y, Fiskum G, Schubert D, 2002 Generation of reactive oxygen species by the mitochondrial electron transport chain. J. Neurochem 80, 780–787. [PubMed: 11948241]

Lovatt D, Sonnewald U, Waagepetersen HS, Schousboe A, He W, Lin JH-C, Han X, Takano T, Wang S, Sim FJ, Goldman S. a, Nedergaard M, 2007 The transcriptome and metabolic gene signature of protoplasmic astrocytes in the adult murine cortex. J. Neurosci 27, 12255–12266. [PubMed: 17989291]

Marrif H, Juurlink BHJ, 1999 Astrocytes respond to hypoxia by increasing glycolytic capacity. J. Neurosci. Res 57, 255–260. [PubMed: 10398303]

Mizushima N, Yoshimori T, 2007 How to interpret LC3 immunoblotting. Autophagy 3, 542–545. [PubMed: 17611390]

Mizushima N, Yoshimori T, Levine B, 2010 Methods in mammalian autophagy research. Cell 140, 313–326. [PubMed: 20144757]

Mozaffarian D, Benjamin EJ, Go AS, Arnett DK, Blaha MJ, Cushman M, de Ferranti S, Despres J-P, Fullerton HJ, Howard VJ, Huffman MD, Judd SE, Kissela BM, Lackland DT, Lichtman JH, Lisabeth LD, Liu S, Mackey RH, Matchar DB, McGuire DK, Mohler ER, Moy CS, Muntner P, Mussolino ME, Nasir K, Neumar RW, Nichol G, Palaniappan L, Pandey DK, Reeves MJ, Rodriguez CJ, Sorlie PD, Stein J, Towfighi A, Turan TN, Virani SS, Willey JZ, Woo D, Yeh RW, Turner MB, 2015 Heart Disease and Stroke Statistics—2015 Update. A Report From the American Heart Association.

Nehlig A, Wittendorp-Rechenmann E, Lam CD, 2004 Selective uptake of [14C]2-deoxyglucose by neurons and astrocytes: high-resolution microautoradiographic imaging by cellular 14C-trajectography combined with immunohistochemistry. J. Cereb. Blood Flow Metab 24, 1004–1014. [PubMed: 15356421]

O'Donnell JC, Jackson JG, Robinson MB, 2016 Transient oxygen/glucose deprivation causes a delayed loss of mitochondria and increases spontaneous calcium signaling in astrocytic processes. J. Neurosci 36, 7109–7127. [PubMed: 27383588]

Ong SB, Subrayan S, Lim SY, Yellon DM, Davidson SM, Hausenloy DJ, 2010 Inhibiting mitochondrial fission protects the heart against ischemia/reperfusion injury. Circulation 121, 2012–2022. [PubMed: 20421521]

Papanicolaou KN, Ngoh GA, Dabkowski ER, O'Connell KA, Ribeiro RF, Stanley WC, Walsh K, 2012 Cardiomyocyte deletion of mitofusin-1 leads to mitochondrial fragmentation and improves tolerance to ROS-induced mitochondrial dysfunction and cell death. Am. J. Physiol. Heart Circ. Physiol 302, H167–H179. [PubMed: 22037195]

Parone PA, Da Druz S, Tondera D, Mattenberger Y, James DI, Maechler P, Barja F, Martinou JC, 2008 Preventing mitochondrial fission impairs mitochondrial function and leads to loss of mitochondrial DNA. PLoS One 3.

Parpura V, Haydon PG, 2000 Physiological astrocytic calcium levels stimulate glutamate release to modulate adjacent neurons. Proc. Natl. Acad. Sci. U. S. A 97, 8629–8634. [PubMed: 10900020]

Paulsen RE, Fonnum F, 1989 Role of glial cells for the basal and Ca2+−dependent K +−evoked release of transmitter amino acids investigated by microdialysis. J. Neurochem 52, 1823–1829. [PubMed: 2566651]

Perez-Campo R, López-Torres M, Cadenas S, Rojas C, Barja G, 1998 The rate of free radical production as a determinant of the rate of aging: evidence from the comparative approach. J. Comp. Physiol. B Biochem. Syst. Environ. Physiol 168, 149–158.

Qi X, Qvit N, Su YC, Mochly-Rosen D, 2013 A novel Drp1 inhibitor diminishes aberrant mitochondrial fission and neurotoxicity. J. Cell Sci 126, 789–802. [PubMed: 23239023]

Risher WC, Croom D, Kirov SA, 2012 Persistent astroglial swelling accompanies rapid reversible dendritic injury during stroke-induced spreading depolarizations. Glia 60, 1709–1720. [PubMed: 22821441]

Rossi DJ, Brady JD, Mohr C, 2007 Astrocyte metabolism and signaling during brain ischemia. Nat. Neurosci 10, 1377–1386. [PubMed: 17965658]

Rothstein JD, Dykes-Hoberg M, Pardo CA, Bristol LA, Jin L, Kuncl RW, Kanai Y, Hediger MA, Wang Y, Schielke JP, Welty DF, 1996 Knockout of glutamate transporters reveals a major role for astroglial transport in excitotoxicity and clearance of glutamate. Neuron 16, 675–686. [PubMed: 8785064]

Rubinsztein DC, Cuervo AM, Ravikumar B, Sarkar S, Korolchuk V, Kaushik S, Klionsky DJ, 2009 In search of an "autophagomometer". Autophagy 5, 585–589. [PubMed: 19411822]

Shih AY, Johnson DA, Wong G, Kraft AD, Jiang L, Erb H, Johnson JA, Murphy TH, 2003 Coordinate regulation of glutathione biosynthesis and release by Nrf2-expressing glia potently protects neurons from oxidative stress. J. Neurosci 23, 3394–3406. [PubMed: 12716947]

Silver IA, Deas J, Erecińska M, 1997 Ion homeostasis in brain cells: differences in intracellular ion responses to energy limitation between cultured neurons and glial cells. Neuroscience 78, 589–601. [PubMed: 9145812]

Sochocka E, Juurlink BHJ, Code WE, Hertz V, Peng L, Hertz L, 1994 Cell death in primary cultures of mouse neurons and astrocytes during exposure to and "recovery" from hypoxia, substrate deprivation and simulated ischemia. Brain Res. 638, 21–28. [PubMed: 8199861]

Solaini G, Harris DA, 2005 Biochemical dysfunction in heart mitochondria exposed to ischaemia and reperfusion. Biochem. J 390, 377–394. [PubMed: 16108756]

Swanson RA, Shiraishi K, Morton MT, Sharp FR, 1990 Methionine sulfoximine reduces cortical infarct size in rats after middle cerebral artery occlusion. Stroke 21, 322–327. [PubMed: 2305410]

Talbot DA, Lambert AJ, Brand MD, 2004 Production of endogenous matrix superoxide from mitochondrial complex I leads to activation of uncoupling protein 3. FEBS Lett. 556, 111–115. [PubMed: 14706836]

Tanida I, Ueno T, Kominami E, 2004 LC3 conjugation system in mammalian autophagy. Int. J. Biochem. Cell Biol 36, 2503–2518. [PubMed: 15325588]

Twig G, Elorza A, Molina AJA, Mohamed H, Wikstrom JD, Walzer G, Stiles L, Haigh SE, Katz S, Las G, Alroy J, Wu M, Py BF, Yuan J, Deeney JT, Corkey BE, Shirihai OS, 2008 Fission and selective

fusion govern mitochondrial segregation and elimination by autophagy. EMBO J. 27, 433–446. [PubMed: 18200046]

Waniewski RA, Martin DL, 1986 Exogenous glutamate is metabolized to glutamine and exported by rat primary astrocyte cultures. J. Neurochem 47, 304–313. [PubMed: 2872273]

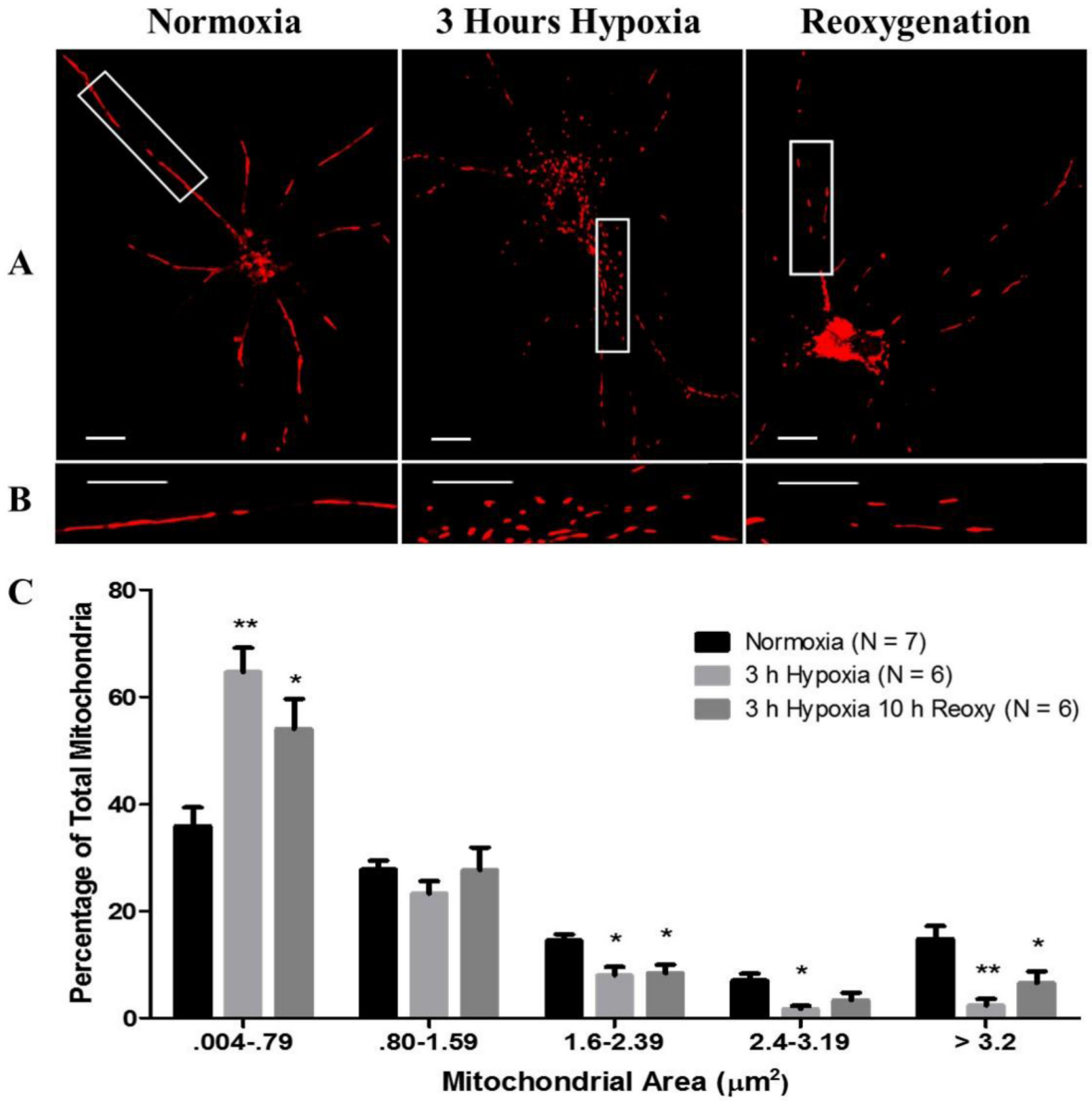

Fig. 1.

Hypoxic exposure induces excessive mitochondrial fission. (A and B) Micrographs depicting a 63× magnification of labeled mitochondria with MitoTracker Red CMXRos (Red) in primary rat astrocytes incubated under normoxia, 3-hours hypoxia and no reoxygenation, and 3-hours hypoxia then 10-hours reoxygenation. Row (B) contains magnified images of row (A). Scale bar 10 μm. Panel (C) contains a bar graph (mean +/− SEM) depicting data of individual mitochondrial area (μm^2) as percent of the total mitochondria per astrocyte for each experimental group; normoxia (n = 550), 3-hours hypoxia (n = 743), 3-hours hypoxia then 10-hours reoxygenation (n = 312). Two-way ANOVA, Bonferroni's multiple comparison test was used to determine the level of significance between the experimental groups: (*$p < 0.05$; **$p < 0.01$). (For interpretation of

the references to colour in this figure legend, the reader is referred to the web version of this article.)

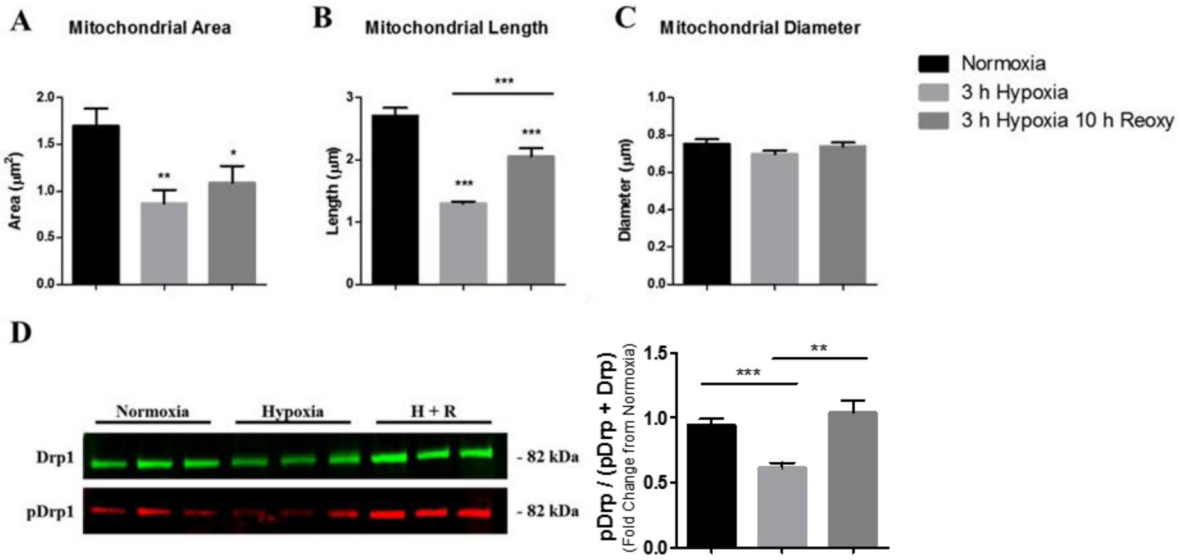

Fig. 2.

Measurements of mitochondria dimensions in astrocytes (A-C) after exposure to hypoxia and post-hypoxia reoxygenation. Bar graph (mean +/− SEM) depicting data of (A) mitochondrial area, (B) mitochondrial length, and (C) mitochondrial diameter as average of total mitochondria per astrocyte for each experimental group; normoxia (n = 550), 3-hours hypoxia (n = 743), 3-hours hypoxia then 10-hours reoxygenation (n = 312). (D) Characterization of Drp-1 phosphorylation after hypoxia and reoxygenation. SDS-PAGE immunoblots indicate a reduced Drp-1 phosphorylation after hypoxic treatment and a subsequent increase with reoxygenation. Western blot analysis of whole cell lysates were determined by anti-pDrp-1 (Ser 637) antibodies (red) and anti-Drp-1 (green) for normoxia (n = 11), 3-hours hypoxia (n = 14), and 3-hours hypoxia then 10-hours reoxygenation (H + R, n = 16). Bar graph (mean +/− SEM) depicting pDrp-1 data as the percentage of total Drp-1. Panels A-C were analyzed with a one-way ANOVA, Bonferroni's multiple comparison test to determine the level of significance between the experimental groups (*$p < 0.05$; **$p < 0.01$; ***$p < 0.0001$). Panel D was analyzed with a one-tailed *t*-test to determine the level of significance between the experimental groups (*$p < 0.05$; **$p < 0.01$). (For interpretation of the references to colour in this figure legend, the reader is referred to the web version of this article.)

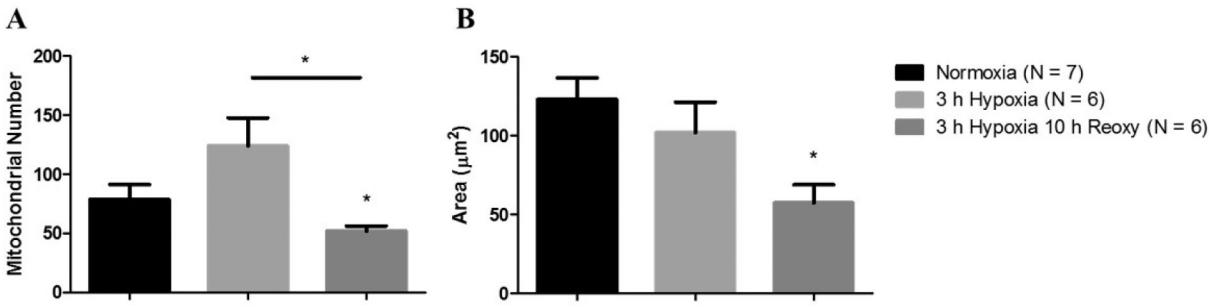

Fig. 3.

Astrocytic mitochondrial content fluctuates in response to hypoxia and reoxygenation. Bar graphs (mean +/− SEM) depicting the average total number of mitochondria per astrocyte (A) and total area (μm^2) occupied by mitochondria per astrocyte (B) for each experimental group, normoxia (left, n = 7), 3-hours hypoxia (center, n = 6), and 3-hours hypoxia then 10-hours reoxygenation (right, n = 6). One-way ANOVA, Bonferroni's multiple comparison test was used to determine the level of significance between the experimental groups (*$p < 0.05$).

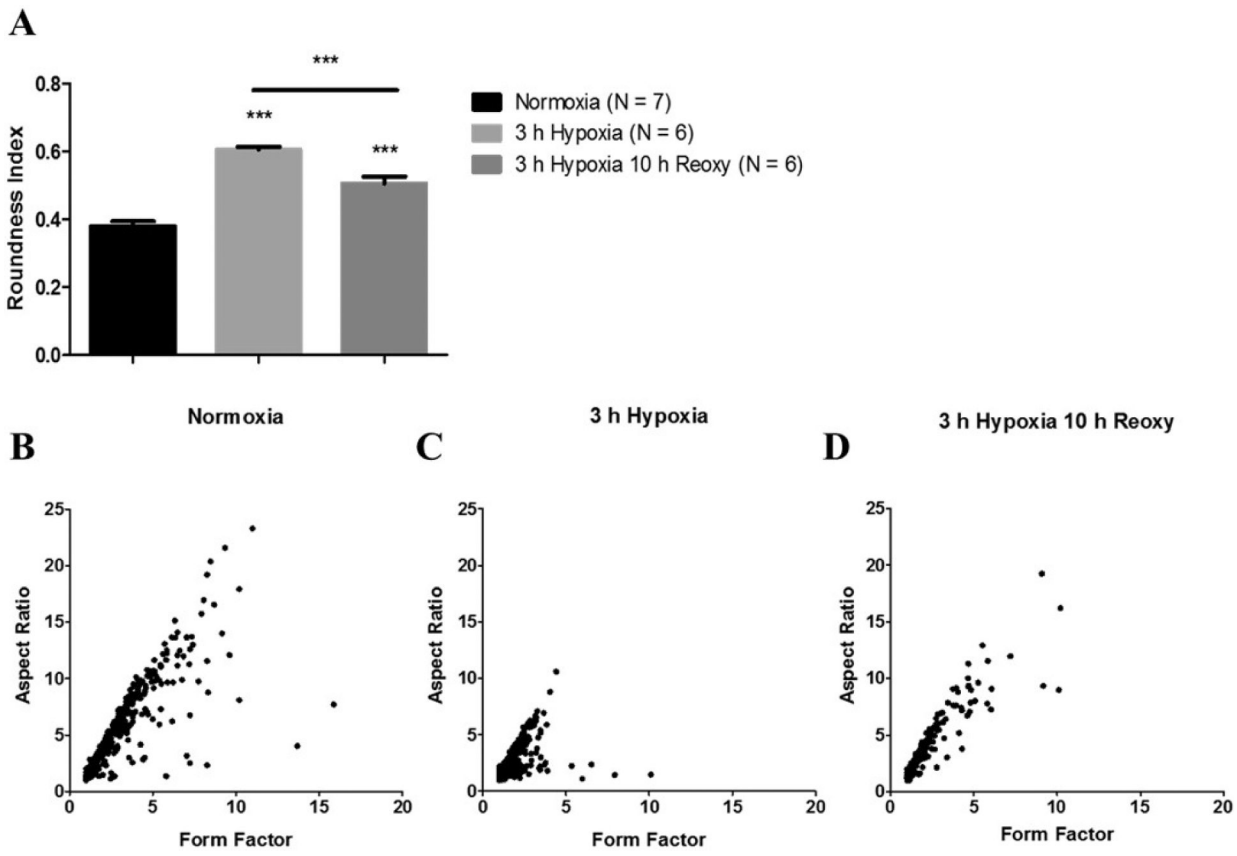

Fig. 4.

Hypoxia induces mitochondrial remodeling into a more rounded morphology and a loss of network complexity. (A) Bar graph depicting roundness values for each experimental group; normoxia (left, n = 550), 3-hours hypoxia (center, n = 743), and 3-hours hypoxia then 10-hours reoxygenation (right, n = 312). (B-D) Scatter plots representing mitochondrial network complexity. Scatter plot of mitochondrial aspect ratio as a function of form factor for (B) normoxia (n = 550), (C) 3-hours hypoxia (n = 743), and (D) 3-hours hypoxia then 10-hours reoxygenation (n = 312). Increasing value of aspect ratio indicates larger size while increasing form factor value indicates greater mitochondrial network complexity. Panel A was analyzed with a one-way ANOVA, Bonferroni's multiple comparison test to determine the level of significance between experimental groups (***$p < 0.0001$).

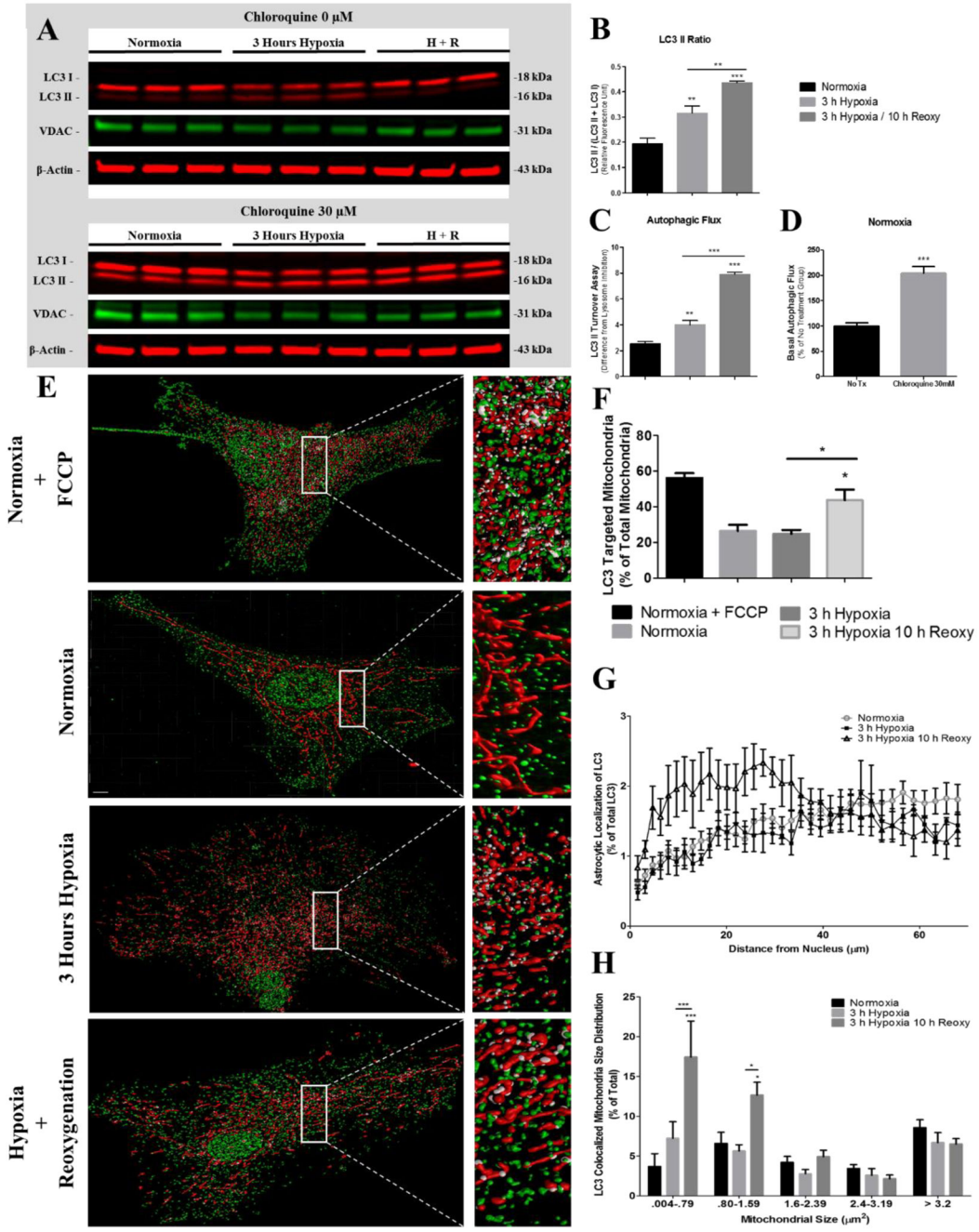

Fig. 5.

Expression and colocalization of LC3 with mitochondria in astrocytes. SDS-PAGE immunoblots indicate an increased LC3 II content after hypoxia and reoxygenation (A) Western blot analysis of whole cell lysates were used to determine the magnitude of (B) LC3 II conversion, (C) cellular VDAC content, (D) autophagic flux, and (E) basal autophagic efficiency. Western blots of lysates from normoxia (n = 5), 3-hours hypoxia (n = 5), and 3-hours hypoxia then 10-hours reoxygenation (H + R, n = 5) were labeled with anti-LC3 (red, green), VDAC (green), and β-actin (red) antibodies. (F) Representative three-dimensional reconstructions of z-stacks depicting mitochondria (red), LC3 (green), and colocalized areas

(white) in astrocytes, incubated at normoxia (FCCP), normoxia, 3-hours hypoxia, and 3-hours hypoxia then 10-hours reoxygenation. Scale bar 10 μm. (G) Bar graph (mean +/− SEM) depicting the percentage of total mitochondria colocalized with LC3 in astrocytes incubated under normoxia (FCCP) (n = 7), normoxia (n = 7), 3-hours hypoxia (n = 5), and 3-hours of hypoxia then 10-hours reoxygenation (n = 6). (H) Bar graph (+/− SEM) depicting percentage of mitochondria colocalized with LC3 as a function of mitochondrial size (μm^2). (I) Line graph depicting the percentage of extranuclear LC3 (+/− SEM) as a function of nuclear distance for astrocytes incubated at normoxia (circle, n = 7), 3-hours hypoxia (square, n = 5), and 3-hours hypoxia then 10-hours reoxygenation (triangle, n = 6). One-way ANOVA, Bonferroni's multiple comparison test was used to determine the level of significance between the experimental groups (*$p < 0.05$; **$p < 0.01$; ***$p < 0.0001$). (For interpretation of the references to colour in this figure legend, the reader is referred to the web version of this article.)

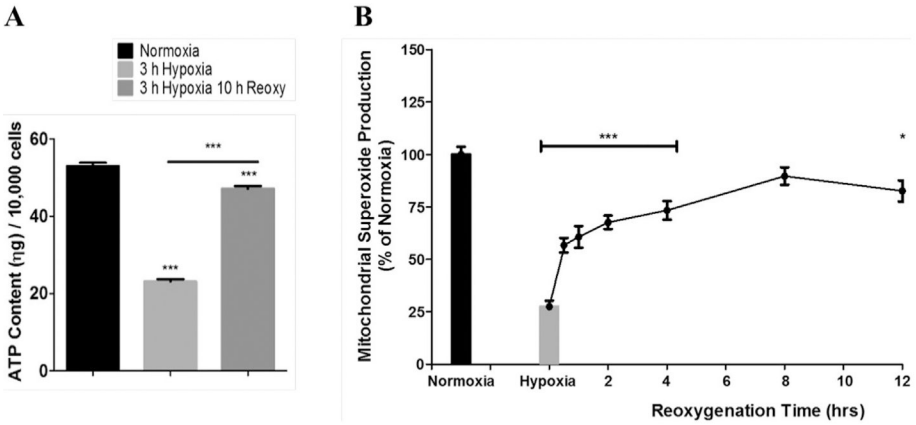

Fig. 6.

Bar graph (mean +/− SEM) depicting astrocytic ATP content (ng) per 10,000 cells for astrocytes incubated under normoxia (n = 18), 3-hours hypoxia (n = 12), and 3-hours hypoxia then 10-hours reoxygenation (n = 24) (A). Mitochondrial superoxide production during normoxia, after hypoxia and throughout post-hypoxia reoxygenation (B). Quasi bar graph and line graph (mean +/− SEM) depicting the time-dependent superoxide production by mitochondria during normoxia (n = 24), hypoxia (n = 21), and for 0.5, 1, 2, 4, 8, and 12-hours reoxygenation (n = 22). Panel A was analyzed by a one-way ANOVA, Bonferroni's multiple comparison test was used to determine the level of significance between the experimental groups (***$p < 0.0001$). Panel B was assessed by one-way ANOVA, Dunnett's post-hoc test was used to determine the level of significance between the experimental groups (*$p < 0.05$; ***$p < 0.0001$).

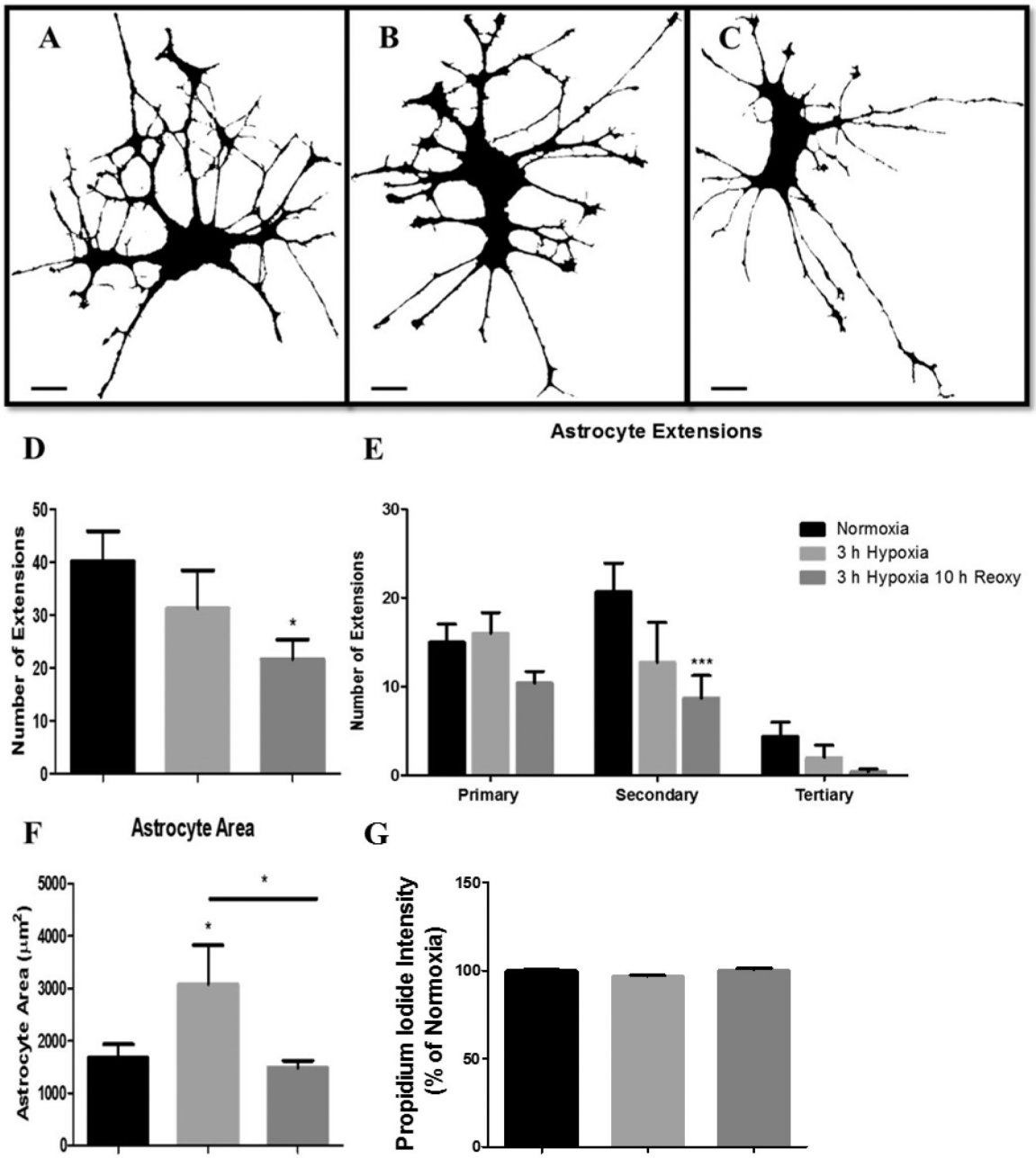

Fig. 7.

Hypoxic exposure and post-hypoxic reoxygenation results in a loss of astrocytic extensions. Confocal micrographs depicting 63× magnification binary images of primary astrocytes incubated under (A) normoxia (n = 7), (B) 3-h hypoxia (n = 5), and (C) 3-hours hypoxia then 10-hours reoxygenation (n = 7). Scale bar 10 μm. (D) Bar graph (mean +/− SEM) depicting total number of astrocytic extensions for each experimental group. (E) Bar graph (mean +/− SEM) depicting the number of astrocytic extensions categorized into primary, secondary, or tertiary extensions per each experimental group. (F) Bar graph (mean +/− SEM) depicting total astrocytic area (μm^2) for each experimental group normoxia (n = 7), 3-hours hypoxia (n = 6), 3-hours hypoxia then 10-hours reoxygenation (n = 6). (G) Bar graph

(mean +/− SEM) depicting cell death indicated by Propidium iodide fluorescence intensity for each experimental group normoxia (n = 24), 3-hours hypoxia (n = 24), 3-hours hypoxia then 10-hours reoxygenation (n = 24). One-way ANOVA, Bonferroni's multiple comparison test was used to determine the level of significance between the experimental groups (*$p < 0.05$; ***$p < 0.0001$).